

# Discovery prospects of Light Higgs at LHC in Type-I 2HDM

---

**Disha Bhatia<sup>a</sup> Ushoshi Maitra<sup>a</sup> Saurabh Niyogi<sup>b</sup>**

<sup>a</sup>*Department of Theoretical Physics, Tata Institute of Fundamental Research, Homi Bhabha Road, Colaba, Mumbai 400 005, India*

<sup>b</sup>*Department of Physics and Astrophysics, University of Delhi, Delhi 110007, India*

*E-mail:* [disha@theory.tifr.res.in](mailto:disha@theory.tifr.res.in), [ushoshi@theory.tifr.res.in](mailto:ushoshi@theory.tifr.res.in),  
[saurabhphys@gmail.com](mailto:saurabhphys@gmail.com)

**ABSTRACT:** We present a comprehensive analysis of observing a Higgs ( $h$ ), lighter than the discovered Higgs in the context of Type-I 2HDM. The decays to  $\gamma\gamma$  and  $b\bar{b}$  serve as the promising channels to probe light Higgs in the mass range of 70-110 GeV at 13/14 TeV LHC. The  $\gamma\gamma$  channel is analyzed in  $ggF$  and  $Wh$  production mode and for  $b\bar{b}$ , associated production of  $h$  with  $W$  and top pairs is considered. Jet substructure techniques are used to suppress the QCD background in the  $b\bar{b}$  channel. The channels  $pp \rightarrow Wh \rightarrow \ell\nu b\bar{b}$  and  $pp \rightarrow h \rightarrow \gamma\gamma$  probe similar parameter space for large  $\tan\beta$  and could be observed with  $\sim 1000 \text{ fb}^{-1}$  of Luminosity. With the similar amount of data,  $pp \rightarrow t\bar{t}h \rightarrow t\bar{t}b\bar{b}$  could be useful in the low  $\tan\beta$  region. However, around the fermiophobic limit, such a light Higgs can be looked for even with a few hundreds  $\text{fb}^{-1}$  of Luminosity in  $pp \rightarrow Wh \rightarrow \ell\nu\gamma\gamma$ .

---

## Contents

<b>1</b>	<b>Introduction</b>	<b>1</b>
<b>2</b>	<b>2HDM: A snippet review</b>	<b>3</b>
<b>3</b>	<b>Promising channels to explore at the LHC</b>	<b>5</b>
<b>4</b>	<b>Experimental constraints</b>	<b>6</b>
4.1	Constraints from flavour data	6
4.2	LEP constraints	7
4.3	LHC Constraints: signal strength measurements of the 125 GeV Higgs	8
4.4	Bounds from scalar searches at the LHC-run 1	9
<b>5</b>	<b>Future prospects at LHC-run2</b>	<b>10</b>
5.1	Reconstructing objects at the LHC	10
5.2	Signal-Background analysis	13
5.2.1	Channel 1: $pp \rightarrow h \rightarrow \gamma\gamma$	13
5.2.2	Channel 2: $pp \rightarrow Wh \rightarrow \ell\nu\gamma\gamma$	15
5.2.3	Channel 3: $pp \rightarrow Wh \rightarrow \ell\nu b\bar{b}$	16
5.2.4	Channel 4: $pp \rightarrow t\bar{t}h \rightarrow t\bar{t}b\bar{b}$	18
<b>6</b>	<b>Discussions and Conclusion</b>	<b>19</b>
<b>7</b>	<b>Acknowledgement</b>	<b>21</b>
<b>A</b>	<b>Cross-section plots</b>	<b>21</b>

---

## 1 Introduction

The recently discovered scalar particle at the Large Hadron Collider (LHC) [1, 2] closely resembles the Higgs boson conjectured in the Standard Model (SM) as its measured couplings with gauge bosons and fermions are in reasonable agreement with the SM predictions [3]. However, there still exists a possibility that the discovered particle may belong to an enlarged scalar sector of a Beyond Standard model scenario (BSM). Usually the additional scalars are considered to be heavy and in some cases decoupled from the low energy effective theory. There exist another scenario where some of the scalars are lighter than the observed Higgs and perhaps are buried beneath the huge SM backgrounds. We explore such a scenario at the LHC in the context of the two Higgs doublet model (2HDM).

The two Higgs doublet model is one of the simplest extension of the SM with an additional  $SU(2)_L$  doublet. The generic structure of 2HDM induces large flavor changing

neutral currents (FCNC) at tree level and faces severe constraints from the experimental data. These FCNC's can be suppressed by imposing a discrete  $Z_2$  symmetry, which further classifies 2HDM into four categories, viz. Type-I, Type-II, flipped and lepton specific [4]. In the process of spontaneously breaking of  $SU(2)_L \times U(1)_Y$  symmetry, three out of eight fields generate masses for  $W$ ,  $Z$  bosons and remaining five physical scalars are: light CP-even Higgs ( $h$ ), Heavy CP-even Higgs ( $H$ ), a pseudoscalar ( $A$ ) and charged Higgs bosons ( $H^\pm$ ).

In most of the analysis [5–10], the lighter CP even Higgs boson ( $h$ ) is identified with the discovered scalar and other scalars ( $H$ ,  $H^\pm$  and  $A$ ) are assumed to be heavy. However, there may exist a scenario where the observed Higgs corresponds to the heavier CP-even scalar i.e.  $H$  with  $m_H = 125$  GeV. In this case,  $h$  is lighter than the observed Higgs. The phenomenology of such light Higgs for all types of 2HDM have been thoroughly studied in the context of vacuum stability, perturbativity, unitarity, electroweak precision measurements, flavor observables and Higgs searches at the colliders [11–18]. Such a scenario is least excluded for the Type-I 2HDM [17, 18] whereas the parameter space of the other 2HDMs (particularly, Type-II) are strongly constrained.

In this manuscript, we search for the light Higgs in the mass range of 70-110 GeV at the LHC. The mass range is chosen to restrict the decay of the observed 125 GeV Higgs to a pair of light Higgs. As a result, the bounds coming from the total decay width measurements of this scalar [19] are irrelevant for our analysis. The light Higgs can be produced via gluon-gluon fusion (ggF), vector boson fusion (VBF) and in association with a  $W/Z$  boson or, a pair of top quarks at the LHC. In most of the parameter space, the light Higgs decays dominantly to  $b\bar{b}$ . However, in certain region, tree level couplings of the light Higgs with fermions vanish and the bosonic decay modes, diphoton in particular, becomes dominant. In this limit, the light Higgs behaves as a fermiophobic scalar (refer to [20] and references therein). We shall see that the interplay of various production channels as well as decay modes provides a complimentary way to explore the entire parameter space. In the diphoton channel, we concentrate on the production of the scalar through gluon fusion and in association with gauge bosons whereas for  $b\bar{b}$  we focus on its production with associated gauge boson/top pair. Owing to a clean environment, the diphoton channel is one of the favorite channels to search for such low mass scalar at the LHC. On the contrary, the  $b\bar{b}$  channel is plagued by huge SM multijet backgrounds at the LHC. In this channel, we consider the light Higgs in the boosted region, where jet substructure techniques can be employed, enabling us to discriminate signal from SM backgrounds [21, 22].

The paper is organized in the following manner. We give a brief introduction of 2HDM in sec. 2. Next, we discuss various plausible channels that can be used to search for the light Higgs at the LHC in sec. 3. We review various constraints arising from low energy experiments and latest results of the LHC Higgs searches in sec. 4. The dedicated collider analysis of the Light Higgs in the allowed parameter space at the LHC is explored in sec. 5. We summarize our results in sec. 6.

## 2 2HDM: A snippet review

The  $Z_2$ -symmetric 2HDM Lagrangian with two  $SU(2)_L$  Higgs doublets ( $\Phi_1$  and  $\Phi_2$ )<sup>1</sup> can be parameterized as [4]:

$$\mathcal{L}_{\text{2HDM}} = (D_\mu \Phi_1)^\dagger D^\mu \Phi_1 + (D_\mu \Phi_2)^\dagger D^\mu \Phi_2 + \mathcal{L}_{\text{Yuk}}(\Phi_1, \Phi_2) - V(\Phi_1, \Phi_2). \quad (2.1)$$

$\mathcal{L}_{\text{Yuk}}$  represents the Yukawa interactions of the doublet with the fermions and  $V(\Phi_1, \Phi_2)$  is the scalar potential comprising of scalar self interactions and is given by,

$$\begin{aligned} V(\Phi_1, \Phi_2) = & m_{11}^2 \Phi_1^\dagger \Phi_1 + \frac{\lambda_1}{2} (\Phi_1^\dagger \Phi_1)^2 + m_{22}^2 \Phi_2^\dagger \Phi_2 + \frac{\lambda_2}{2} (\Phi_2^\dagger \Phi_2)^2 - m_{12}^2 \Phi_1^\dagger \Phi_2 \\ & + \lambda_3 \Phi_1^\dagger \Phi_1 \Phi_2^\dagger \Phi_2 + \lambda_4 \Phi_1^\dagger \Phi_2 \Phi_2^\dagger \Phi_1 - \frac{1}{2} \lambda_5 (\Phi_1^\dagger \Phi_2)^2 + h.c., \end{aligned} \quad (2.2)$$

where,

$$\Phi_1 = \begin{pmatrix} \phi_1^+ \\ \frac{1}{\sqrt{2}} [\rho_1 + i\eta_1 + v_1] \end{pmatrix}, \quad \Phi_2 = \begin{pmatrix} \phi_2^+ \\ \frac{1}{\sqrt{2}} [\rho_2 + i\eta_2 + v_2] \end{pmatrix}. \quad (2.3)$$

$m_{12}$  is the  $Z_2$  symmetry breaking parameter in the potential and  $v_1^2 + v_2^2 = v^2$ . The spontaneous symmetry breaking of  $SU(2)_L \times U(1)_Y$  results into five physical scalar fields— $h$ ,  $H$ ,  $A$  and  $H^\pm$  and three Goldstone bosons— $G$ ,  $G^\pm$  which are absorbed as the longitudinal modes for  $Z$  and  $W$  gauge bosons. The mass spectrum of the particles can be worked out by solving eq. (2.2),

$$m_A^2 = \left( \frac{m_{12}^2}{v_1 v_2} - 2\lambda_5 \right) v^2, \quad m_{H^\pm}^2 = m_A^2 + (\lambda_5 - \lambda_4) v^2, \quad (2.4)$$

$$\begin{pmatrix} m_h^2 \\ m_H^2 \end{pmatrix} = \mathcal{R} \begin{pmatrix} m_{12}^2 \tan \beta + \lambda_1 v_1^2 & -m_{12}^2 + (\lambda_3 + \lambda_4 + \lambda_5) v_1 v_2 \\ -m_{12}^2 + (\lambda_3 + \lambda_4 + \lambda_5) v_1 v_2 & m_{12}^2 \cot \beta + \lambda_2 v_1^2 \end{pmatrix} \mathcal{R}^T \quad (2.5)$$

where,  $\mathcal{R}$  is the rotation matrix diagonalizing the CP-neutral Higgs mass matrix and is given by

$$\begin{pmatrix} \sin \alpha & -\cos \alpha \\ -\cos \alpha & -\sin \alpha \end{pmatrix} \quad (2.6)$$

The doublets ( $\Phi_1$  and  $\Phi_2$ ) in terms of the physical fields and the Goldstone bosons are

$$\begin{aligned} \Phi_1 = & \begin{pmatrix} G^+ \cos \beta + H^+ \sin \beta \\ \frac{1}{\sqrt{2}} [h \sin \alpha - H \cos \alpha + i(G \cos \beta + A \sin \beta) + v_1] \end{pmatrix}, \\ \Phi_2 = & \begin{pmatrix} G^+ \sin \beta - H^+ \cos \beta \\ \frac{1}{\sqrt{2}} [-h \cos \alpha - H \sin \alpha + i(G \sin \beta - A \cos \beta) + v_2] \end{pmatrix}, \end{aligned} \quad (2.7)$$

where  $\beta$  diagonalizes the mass matrices for charged Higgs and the CP-odd Higgs ( $\tan \beta = v_2/v_1$ ).

The parameters of the scalar potential ( $m_{11}$ ,  $m_{22}$ ,  $\lambda_i$ ) given in eq. (2.2) can be expressed in terms of seven physical parameters viz. rotation angles ( $\alpha, \beta$ ),  $Z_2$  symmetry breaking

---

<sup>1</sup>Under  $Z_2$  transformation,  $\Phi_1 \rightarrow \Phi_1$  and  $\Phi_2 \rightarrow -\Phi_2$

parameter ( $m_{12}$ ) and masses of the scalars. The parameters are chosen in accordance with the unitarity, vacuum stability and perturbative bounds [4]. The theoretical consistency of the parameter space is validated using 2HDMC [23]. Lower values of  $m_{12}$  are suitable to get  $m_H = 125$  GeV [18]. We therefore fix  $m_{12}^2 = 1000$  GeV<sup>2</sup>.

In Type-I models, fermions couple only to one of the doublets i.e.  $\Phi_2$ ,  $\mathcal{L}_{\text{Yuk}}$  in the unitary gauge is given as [4]

$$\begin{aligned}\mathcal{L}_{\text{Yuk}}^{\text{Type-I}} &= \overline{Q}_L^i \mathcal{Y}_{1ij}^d \Phi_2 d_R^j + \overline{Q}_L^i \mathcal{Y}_{1ij}^u \Phi_2^c u_R^j + \overline{Q}_L^i \mathcal{Y}_{1ij}^e \Phi_2^c e_R^j + h.c. , \\ &= - \sum_{f=u,d,\ell} \frac{m_f}{v} \left( \xi_h^f \bar{f} f h + \xi_H^f \bar{f} f H - i \xi_A^f \bar{f} \gamma_5 f A \right) \\ &\quad - \frac{\sqrt{2} V_{ud}}{v} \bar{u} \left( m_u \xi_A^u P_L + m_d \xi_A^d P_R \right) - \frac{\sqrt{2}}{v} \xi_A^\ell \bar{\nu}_L \ell_R H^+ + h.c. .\end{aligned}\quad (2.8)$$

where  $V_{ud}$  is the CKM matrix element,  $m_f$  is the mass of a fermion,  $f$  and

$$\begin{aligned}\xi_h^{u,d,\ell} &= \cos \alpha / \sin \beta , \quad \xi_H^{u,d,\ell} = \sin \alpha / \sin \beta , \\ \xi_A^u &= \cot \beta , \quad \xi_A^{d,\ell} = -\cot \beta .\end{aligned}\quad (2.9)$$

Substituting eqn. (2.7) in eqn. (2.1), we can obtain the tree-level couplings of  $h$ ,  $H$ ,  $A$  and  $H^+$  with massive gauge bosons. We list a few essential couplings here [24].

$$\begin{aligned}\mathcal{L}_{V-H} &= \frac{m_Z^2}{v} \xi_h^V Z_\mu Z^\mu h + \frac{m_Z^2}{v} \xi_H^V Z_\mu Z^\mu H + 2 \frac{m_W^2}{v} \xi_h^V W_\mu W^\mu h + 2 \frac{m_W^2}{v} \xi_H^V W_\mu W^\mu H \\ &\quad + \frac{g \xi_h^V}{2 \cos \theta_W} (p_h^\mu + p_A^\mu) Z_\mu A h - \frac{g \xi_h^V}{2 \cos \theta_W} (p_H^\mu + p_A^\mu) Z_\mu A H \\ &\quad - \frac{i g \cos 2\theta_W}{2 \cos \theta_W} (p_{H^+}^\mu + p_{H^-}^\mu) Z_\mu H^+ H^- - i e (p_{H^+}^\mu + p_{H^-}^\mu) A_\mu H^+ H^-\end{aligned}\quad (2.10)$$

where

$$\xi_h^V = \sin(\beta - \alpha) \quad , \quad \xi_H^V = \cos(\beta - \alpha) . \quad (2.11)$$

The effective Lagrangian for the loop induced couplings of the scalars with massless gauge bosons is

$$\begin{aligned}\mathcal{L}_{\gamma\gamma(\text{gg})-H} &= \frac{\alpha_s}{8\pi v} G_{\mu\nu}^a G^{a\mu\nu} \left( \xi_h^f F_{1/2}(\tau_f) h + \xi_H^f F_{1/2}(\tau_f) H \right) \\ &\quad + \frac{\alpha_e}{8\pi v} F_{\mu\nu} F^{\mu\nu} \left( \xi_h^f \frac{4}{3} F_{1/2}(\tau_f) + \xi_h^V F_1(\tau_W) \right) h \\ &\quad + \frac{\alpha_e}{8\pi v} F_{\mu\nu} F^{\mu\nu} \left( \xi_H^f \frac{4}{3} F_{1/2}(\tau_f) + \xi_H^V F_1(\tau_W) \right) H \\ &\quad + \frac{\alpha_e}{4\pi v} F_{\mu\nu} \tilde{F}^{\mu\nu} \left( \xi_A^f \frac{4}{3} F_{1/2}(\tau_f) \right) A + \frac{\alpha_s}{4\pi v} G_{\mu\nu}^a \tilde{G}^{\mu\nu a} \left( \xi_A^f F_{1/2}(\tau_f) A \right)\end{aligned}\quad (2.12)$$

For clarity we will use the notation,

$$\xi_h^\gamma = \xi_h^f \frac{4}{3} F_{1/2}(\tau_f) + \xi_h^V F_1(\tau_W) \quad \text{and} \quad \xi_H^\gamma = \xi_H^f \frac{4}{3} F_{1/2}(\tau_f) + \xi_H^V F_1(\tau_W) , \quad (2.13)$$

where,  $F_{1/2}(\tau_f)$  and  $F_1(\tau_f)$  are the top and W loop contribution respectively and are given as

$$\begin{aligned}
F_{1/2}(\tau_t) &= \tau_t(1 + (1 - \tau_t)f(\tau_t)) \text{ and } F_1(\tau_W) = [2 + 3\tau_W + 3\tau_W(2 - \tau_W)f(\tau_W)] \\
f(\tau) &= \left( \sin^{-1} \frac{1}{\sqrt{\tau}} \right)^2 \text{ (for } \tau > 1), \\
f(\tau) &= -\frac{1}{4} \left( \log \frac{\eta_+}{\eta_-} - i\pi \right)^2 \text{ (for } \tau < 1), \\
\eta_{\pm} &= 1 \pm \sqrt{1 - \tau}, \quad \tau_i = \left( \frac{2m_i}{m_S} \right)^2, S = h, H.
\end{aligned} \tag{2.14}$$

We identify  $H$  as the observed Higgs boson with  $m_H = 125$  GeV. Its couplings with fermions and gauge bosons are different from that of the SM by the factors  $\xi_H^f$  and  $\xi_H^V$ . In the limit  $\alpha \rightarrow \beta$ ,  $\xi_H^f \rightarrow 1$  and  $\xi_H^V \rightarrow 1$ , the couplings of  $H$  exactly matches with the SM Higgs. This limit in the literature is termed as the alignment limit [4]. In the strict alignment limit, the tree level couplings of light Higgs,  $h$  with the gauge bosons vanishes and couplings with fermions are proportional to  $\cot \beta$ . In this limit the light higgs behaves as fermiophilic. It can be seen from eqn. (2.9) that in the limit  $\alpha \rightarrow \pi/2$ , the couplings of the light Higgs with fermions ( $\xi_h^f$ ) vanish and it behaves as a fermiophobic scalar.

### 3 Promising channels to explore at the LHC

In this section, we discuss the possible modes of production and decay of the light Higgs ( $h$ ). The direct production of the light Higgs boson at the LHC proceeds through the gluon fusion (ggF), vector boson fusion (VBF), associated production of the Higgs with gauge bosons ( $Vh$ ) and in association with top pairs ( $tth$ ). In the left panel of fig. 1, we plot the ratio of production cross section of the light Higgs with that of the SM-like Higgs ( $h_{\text{SM}}$ ) as a function of  $\alpha$ . Here by SM-like Higgs, we mean that its couplings are same as that of the SM-Higgs but with  $m_{h_{\text{SM}}} = m_h$ . The gluon fusion as well as associated top pair production rate of the light Higgs in Type-I model scale as  $(\xi_h^f)^2$  with respect to the SM-like Higgs. Similarly, light Higgs produced in association with gauge bosons or through vector boson fusion, scales as  $(\xi_h^V)^2$ . The scaling has been illustrated in the left panel of the fig. 1. In the right panel, the branching fractions of the light Higgs as a function of  $\alpha$  are shown. In most of the parameter space, the light Higgs decays dominantly to a pair of bottom quarks. Analyzing this channel in the ggF or VBF mode is difficult due to the presence of large QCD background. Demanding additional leptons in the final state from the associated production of the light Higgs with a W/Z or top pair helps to bypass the backgrounds. The branching ratio of the light Higgs to  $\tau$  pair is also significant. However the reconstruction of  $\tau$ 's involve subtle issues due to presence of missing energy, which makes it more suitable as a confirmatory channel rather than the discovery. The parameter space spanned by  $\tau\bar{\tau}$  is exactly same as that of  $b\bar{b}$  (as shown in the right panel of the fig. 1), we therefore restrict ourselves to the analyses of  $b\bar{b}$ .

The diphoton channel is one of the cleanest signal to discover Higgs at LHC. In the fermiophobic limit i.e.  $\alpha = \pi/2$ , the decay of  $h$  to  $\gamma\gamma$  becomes prominent and can only be

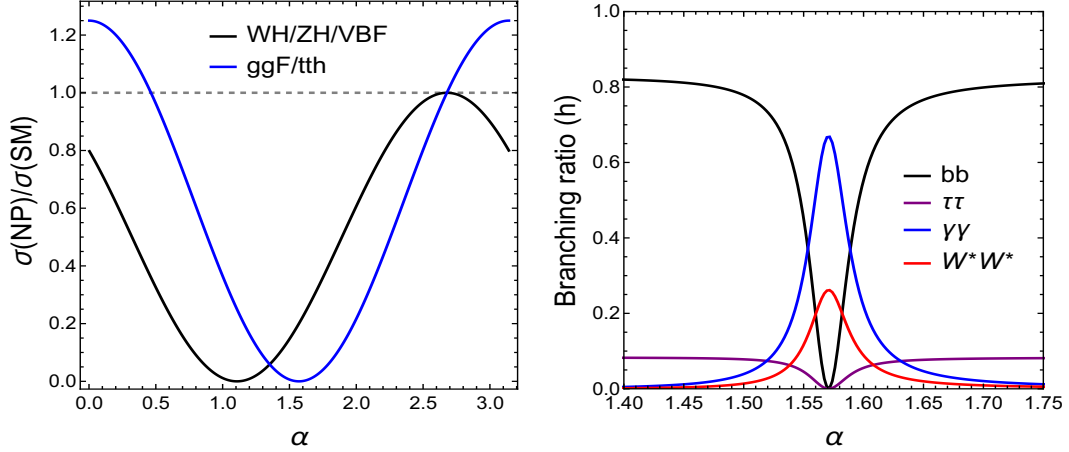


**Figure 1:** A representative plot for  $m_h = 80$  GeV and  $\tan \beta = 2$ . In the left panel, we plot the ratio of cross-sections of the light Higgs ( $h$ ) and the SM-like Higgs ( $h_{\text{SM}}$ ) with respect to  $\alpha$ . In the right panel, the variation of branching ratios of the light higgs with  $\alpha$  are shown (range of  $\alpha$  is restricted near  $\pi/2$  to signify the behaviour around the fermiophobic limit).

probed in the  $Vh$ /VBF channel (as shown in fig. 1). Regions away from the fermiophobic limit can be searched using  $ggF/tth$  mode. The parameter space probed by  $tth$  is identical to gluon fusion. However, its production cross section is roughly 100 times smaller than  $ggF$ , hence we do not consider this mode for diphoton analyses.

Therefore, we have considered the following channels for our analysis:  $gg \rightarrow h \rightarrow \gamma\gamma$ ,  $Vh \rightarrow V\gamma\gamma$ ,  $Vh \rightarrow Vb\bar{b}$  and  $tth \rightarrow t\bar{t}b\bar{b}$ <sup>2</sup>.

## 4 Experimental constraints

In this section, we discuss the bounds on the parameter space arising from flavour observables and measurements at large electron-positron collider (LEP) and LHC.

### 4.1 Constraints from flavour data

The additional scalars can affect the flavor processes like  $B_s \rightarrow X_s \gamma$  or  $B_s \rightarrow \mu\mu$ . Although tree-level FCNC's in 2HDM are absent due to  $Z_2$  symmetry, the neutral and charged scalars can affect these processes through higher order diagrams. In general, the flavor observables in these models are sensitive to the  $m_{H^\pm}$  and  $\tan \beta$ . Usually heavy charged Higgs is preferred as its contribution to FCNC processes are negligible because of loop suppression. For Type-I model, the couplings of the charged Higgs to fermions are anyway suppressed for  $\tan \beta > 2$  and hence, almost all values of  $m_{H^\pm}$  are allowed [25]. The bounds on the parameter space have been verified using **SuperIso** [26].

<sup>2</sup>Parameter space probed by VBF is same to  $Vh$

## 4.2 LEP constraints

In our case T-parameter receives largest contributions and hence, put the most stringent bound. T-parameter in Type-I 2HDM forces  $m_A \approx m_{H^\pm}$  for  $m_{H^\pm} \gtrsim 200$  GeV and for  $m_{H^\pm} \lesssim 200$  GeV, the pseudoscalar mass is unconstrained. The results have been cross-checked using 2HDMC [23]. We now discuss the bounds obtained from the direct detection of scalars at LEP.

- **Charged Higgs searches:** The charged Higgs has been looked for in the channel  $e^+e^- \rightarrow H^+H^-$ . The relevant coupling of this process is independent of any NP parameter (eqn. (2.10)). The null observation of signal in this channel has put a lower bound of 80 GeV on mass of the charged Higgs [27].
- **Light scalar searches:** The light CP-even scalar has been searched in the channel  $e^+e^- \rightarrow Zh$  [28]. The cross-section scales by  $(\xi_h^V)^2$  i.e.  $\sin(\beta - \alpha)^2$  (see eqn. (2.10)). The absence of any excess in this process has put severe constraint on  $|\sin(\beta - \alpha)|$ . The heavier masses are less constrained than the lighter ones due to phase space suppression as the center of mass energy at LEP was limited upto 209 GeV. We have plotted the allowed regions of  $|\sin(\beta - \alpha)|$  with respect to the mass of the light Higgs in fig. 2.

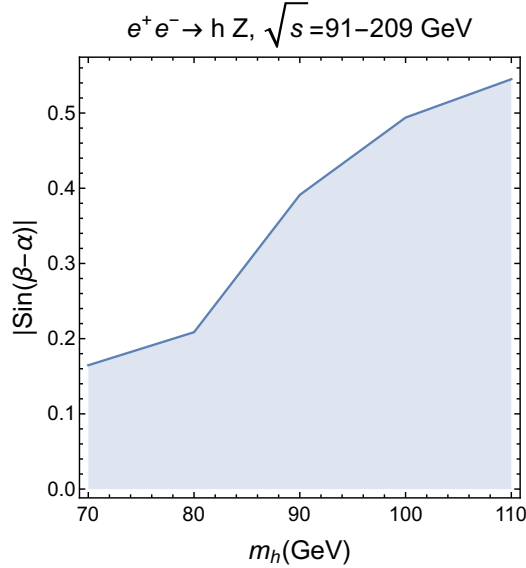


**Figure 2:** The shaded region in the plane of  $(m_h, |\sin(\beta - \alpha)|)$  is allowed by LEP.

LEP-II has searched for  $e^+e^- \rightarrow hA \rightarrow b\bar{b}\gamma\gamma$  that provides a lower bound of 180 GeV on the sum of masses of the light pseudoscalar and light Higgs in the fermiophobic ( $\alpha \rightarrow \pi/2$ ) limit [29]. In the rest of the paper, we assume charged Higgs and pseudoscalar to be decoupled<sup>3</sup>.

<sup>3</sup>A light pseudoscalar having same mass as the light Higgs ( $m_h = m_A$ ) can interfere with the light Higgs



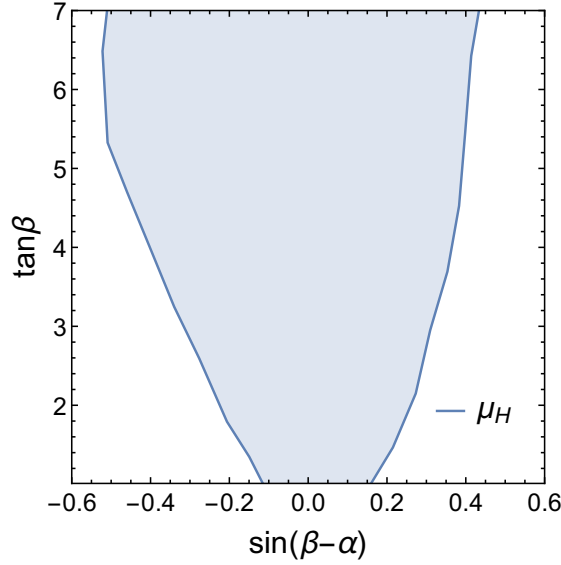


**Figure 3:** The shaded region in the plane of  $(\sin(\beta - \alpha), \tan \beta)$  is allowed from the signal strength measurements of the observed. Note that our result is consistent with [18].

### 4.3 LHC Constraints: signal strength measurements of the 125 GeV Higgs

Signal strength ( $\mu$ ) measurements are used to constrain the couplings of various BSM scenarios. In this section, we discuss the constraints arising from these measurements on the couplings of the heavier CP-even Higgs (H) which we have identified with the observed Higgs. If the observed Higgs is produced through channel  $i$  and decays to  $j$ , then the signal strength ( $\mu_j^i$ ) assuming narrow width approximation is defined as [3, 30],

$$\mu_j^i = \mu^i \mu_j, \quad (4.1)$$

where

$$\mu^i = \frac{\sigma(i \rightarrow H)}{\sigma(i \rightarrow H_{\text{SM}})}, \quad \mu_j = \frac{\text{BR}(H \rightarrow j)}{\text{BR}(H_{\text{SM}} \rightarrow j)}.$$

In Table. 1, we list the effective signal strengths corresponding to the channels of H. The scaling factors  $\xi_H$  are defined in eqns. (2.9), (2.10), (2.13). Note that these factors are exact only at the leading order. However, the deviations after including the higher order corrections are small [18] and we neglect them in our analysis. Signal strength measurements of the observed Higgs force us to be close to alignment limit i.e.,  $\xi_H^V \rightarrow 1$ . The region of the parameter space consistent with the signal strength measurements of 125 GeV scalar [3] is shown in  $(\sin(\beta - \alpha), \tan \beta)$  plane in fig. 3.  $|\sin(\beta - \alpha)| > 0.2$  is ruled out for  $\tan \beta < 2$  as can be seen in fig. 3. The region near  $\alpha \sim \beta$  (alignment limit) is favored for all values of  $\tan \beta$  as  $H$  behaves like the SM-like Higgs in this limit. The allowed range

---

and enhance the cross section in  $b\bar{b}$  mode produced in association with  $t\bar{t}$ . We found that the enhancement in the cross section due to such interference is not significant.

	$f\bar{f}$	$VV^*$	$\gamma\gamma$
ggF/ttH	$(\xi_H^f)^4$	$(\xi_H^f)^2(\xi_H^V)^2$	$(\xi_H^f)^2(\xi_H^\gamma)^2$
VBF/VH	$(\xi_H^V)^2(\xi_H^f)^2$	$(\xi_H^V)^4$	$(\xi_H^V)^2(\xi_H^\gamma)^2$

**Table 1:** The  $ij^{\text{th}}$  element of the table is defined as  $\mu_j^i \times \Sigma_k(\xi_H^k)^2 \text{BR}(H_{\text{SM}}^{125} \rightarrow k)$ . The summation is over  $k$  where  $k$  denotes all possible decay modes of H.

of  $\sin(\beta - \alpha)$  increases with  $\tan\beta$ . When  $\sin(\beta - \alpha) > 0$ ,  $\xi_H^f$  decreases and  $\mu_{ggF}^{125}$  drops beyond the allowed range. When  $\sin(\beta - \alpha) < 0$ ,  $\xi_H^V$  decreases and  $\xi_H^f$  increases. The large destructive interference of top and W loop (See eqn. 2.13) decreases  $\xi_H^H$  and hence,  $\mu_H^\gamma$  reduces below the allowed range. For higher value  $\tan\beta$ , the amount of destructive interference decreases as  $\xi_H^f$  increases and  $\mu_H^\gamma$  lies within the allowed range of  $\mu_{\gamma\gamma}^{125}$ . As a result, negative values of  $\sin(\beta - \alpha)$  is slightly preferred over positive values.

#### 4.4 Bounds from scalar searches at the LHC-run 1

	$f\bar{f}$	$VV^*$	$\gamma\gamma$
ggF/tth	$(\xi_h^f)^4$	$(\xi_h^f)^2(\xi_h^V)^2$	$(\xi_h^f)^2(\xi_h^\gamma)^2$
VBF/Vh	$(\xi_h^V)^2(\xi_h^f)^2$	$(\xi_h^V)^4$	$(\xi_h^V)^2(\xi_h^\gamma)^2$

**Table 2:** The  $ij^{\text{th}}$  element of the table is defined as  $\sigma_j^{h,i} \times \Sigma_k(\xi_h^k)^2 \text{BR}(h_{\text{SM}} \rightarrow k)$ .  $\sigma_j^{h,i}$  represents the production cross section of SM-like Higgs (with mass  $m_h$ ) in  $i^{\text{th}}$  channel times its branching ratio in  $j^{\text{th}}$  channel. The summation is over  $k$  where  $k$  denotes all possible decay modes of h.

In Table. 2, we list the effective scaling of the cross section corresponding to the channels of lighter Higgs ( $h$ ). The LHC has searched for an additional scalar with mass 80 GeV to 110 GeV in the diphoton channel [31, 32]. Absence of any excess over SM backgrounds in this channel can be translated into the bounds on the maximum cross section allowed for a given mass of  $h$ . Figure 4 represents the parameter space in  $\alpha$  vs  $\tan\beta$  plane for Type-I scenario. The blue band in fig. 4 represents the allowed region from the signal strength measurements at the LHC. The orange (green) band is the allowed from the direct search of light Higgs of mass 90 (80) GeV at LEP and LHC. In particular, the wedge-like region at  $\alpha \sim \pi/2$  is disallowed in the  $\gamma\gamma$  final state at the LHC, which is the so-called fermiophobic region. As  $\tan\beta$  increases further, the value of  $\sin(\beta - \alpha)$  decreases that suppresses the production of the light Higgs in  $Vh$ /VBF channel. Note

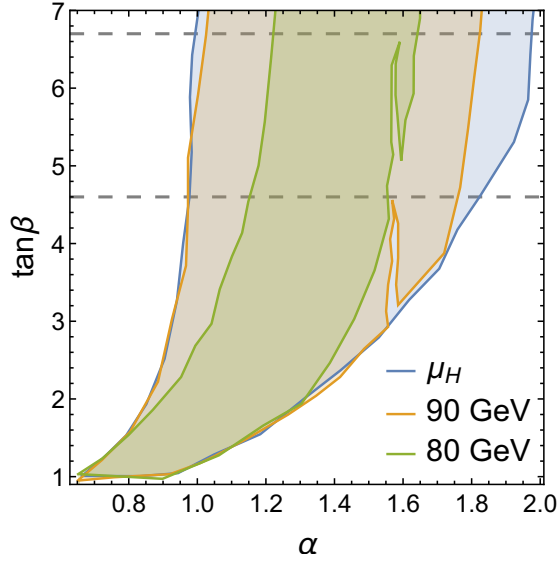


**Figure 4:** The allowed parameter for Type-I 2HDM obtained from the requirement of the heavy Higgs at 125 GeV is shown in blue. The constraints from the non-observation of a light Higgs is also shown. The region in orange (green) is allowed at 95% C.L. from  $VBF/VH \rightarrow \gamma\gamma$  for a light Higgs of 90 (80) GeV. It is interesting to note that the disallowed region from  $VBF/VH \rightarrow \gamma\gamma$  is for  $\alpha \sim \pi/2$ .

that, with increase in the mass of the light Higgs,  $Vh/VBF$  production rate decreases and diphoton searches in associated Higgs channel become insensitive and does not constrain any additional parameter space.

## 5 Future prospects at LHC-run2

As discussed in sec. 3, we consider light Higgs decays to  $b\bar{b}$  and  $\gamma\gamma$ . The  $b\bar{b}$  mode is the dominant decay channel of the light Higgs in most of the parameter space except near the fermiophobic limit ( $\alpha \sim \pi/2$ ) where the decay to diphoton dominates (see fig. 1). We consider associated production of the light Higgs with gauge bosons and top pair for the  $b\bar{b}$  mode. The gluon fusion as well as associated gauge boson production mechanisms of light Higgs are considered for the diphoton channel. While the associated gauge boson production helps to probe the fermiophobic limit, the gluon fusion is suitable for probing regions where  $\sin(\beta - \alpha) < 0$  (See eqn. 2.13). In this section, we shall see that the complementary effect of these two decay modes will allow us to explore the parameter space in a robust way. Next, we discuss the particle identification and reconstruction prescription at the LHC.

### 5.1 Reconstructing objects at the LHC

The signal as well as the SM background processes at the parton level are generated using event generators listed in the Table 3. The generated events are then showered and

hadronized in PYTHIA 8 [33, 34]. Major SM processes, such as,  $t\bar{t} + n$  jets and  $W/Z + n$  jets are generated in MadGraph [35] with proper matching between matrix element and parton shower (ME+PS) [36] in PYTHIA. To carry out realistic simulation, we incorporate detector

Channel	Pythia	Madgraph
$\gamma\gamma$ (Signal)	ggF, $Wh$ , VBF	—
$\gamma\gamma$ (background)	$j\gamma$ , $\gamma\gamma$ , $e^+e^-$	$\ell\nu\gamma\gamma$ , $\ell\nu j\gamma$
$b\bar{b}$ (Signal)	$Wh$	$t\bar{t}h$
$b\bar{b}$ (Background)	$t\bar{t}$	$W/Z + n$ jets , $t\bar{t} + n$ jets , $\ell\nu b\bar{b}$ , $t\bar{t}b\bar{b}$

**Table 3:** Event generators used for analysis.

resolution effects while identifying final state objects.

- **Photons:** The photons are identified from the energy deposits at ECAL. The granularity of the ECAL cells is approximately  $0.02 \times 0.02$  in the  $\eta - \phi$  direction for both the detectors. However, due to the electromagnetic shower generated by photons, a photon candidate is contained within a  $5 \times 5$  crystal matrix around the seed i.e the actual hit point of a particular ECAL cell. This amounts to  $\Delta R \approx 0.09$  ( $\Delta R^2 = \Delta\eta^2 + \Delta\phi^2$ ). Thus the photon candidates are not point like objects, but rather have a finite spread. The momentum of the photon candidate is defined as the vector sum of all ECAL deposits within the cone of  $\Delta R$  around the seed. We select photon candidates with transverse momentum  $p_T > 20\text{GeV}$  and pseudorapidity  $|\eta| < 2.5$  (owing to the finite resolution size of the ECAL). Photon associated with any QCD process, like ( $\pi^0 \rightarrow \gamma\gamma$ ) will have large jet activity around it. To get rid of such events, we demand photons to be isolated. The photon candidates are considered isolated if the total scalar sum of the transverse energy of other objects within the cone of  $\Delta R_{\text{iso}} = 0.4$  is less than 10% of the  $p_T$  of the candidate photon. We have taken into account a typical 5% probability for an electron to fake a photon due to track mis-measurements in our simulation.
- **Leptons:** We select electrons (muons) with  $p_T > 20\text{ GeV}$  and within the pseudorapidity region  $|\eta| < 2.5$  (2.7). While electron isolation criteria is similar to that of the photon, for muons we demand scalar sum of hadronic energy to be less than 25% of muon  $p_T$ .
- **Missing Transverse energy:** The missing transverse energy ( $E_T^{\text{miss}}$ ) is defined as the negative of vector sum of total visible transverse momentum. In our analysis, we have considered all visible particles with  $p_T > 0.5\text{ GeV}$ .
- **Jets:** We have reconstructed  $R = 0.4$  jets using anti-Kt [37] algorithm with  $p_T^j > 30\text{ GeV}$  and  $|\eta| < 4.5$ . The typical momentum transfer at 14 TeV center-of-mass

energy is quite high and the daughter particles are much boosted. Therefore, there could be instances when the decay products of the parent (P) such as Higgs/top quark are collimated and can be encompassed within a single jet of larger cone size, usually called a fat jet. The Higgs and tops are then identified by using substructure information of the fat jet. We consider jets of radius ( $\Delta R > 0.8$ ) reconstructed using **FastJet** [38] with Cambridge-Aachen (CA) algorithm [39]. The angular separation of the decay products can be estimated roughly as  $\Delta R = 2m_P/p_T^P$ . To resolve the angular scale of the fat jet, CA algorithm is preferred over anti-kT as it provides hierarchial structure of the clustering in angles. We have considered 70% tagging efficiency for a b-jet.

- **Higgs:** In the  $\gamma\gamma$  channel, reconstruction of Higgs is rather simple as opposed to  $b\bar{b}$  due to large multi-jet background. In case of  $b\bar{b}$ , if the Higgs is produced with large  $p_T$ , then the decay products can be enclosed within a single fat jet (J). We identify a fat jet with  $p_T^J > 150$  GeV and  $\Delta R_{CA}$  varying from 0.8 to 1.2 as Higgs using the following MASSDROP technique [21]:
  - The fatjet (J) is broken into two subjets ( $j_1$  and  $j_2$ ) such that  $m_{j_1} > m_{j_2}$  and  $m_{j_1}, m_{j_2} > 30$  GeV.
  - The two subjets are considered if  $m_{j_1} < \mu m_J$  and the splitting  $y = \frac{\min(p_{t_{j_1}}^2, p_{t_{j_2}}^2) \Delta R_{j_1 j_2}^2}{m_j^2}$  is not too asymmetric i.e  $y > y_{cut}$ . Typically,  $\mu = 0.67$  and  $y_{cut} = 0.09$ .
  - If the previous condition is not satisfied then  $j_1$  is considered instead of J till both the conditions are satisfied.
  - The final jet is considered as Higgs if both the subjets are b-tagged and mass of the filtered<sup>4</sup> fat jet ( $m_J$ ) is close to the Higgs mass.
- **Top:** The hadronic decay of top is generally characterized by three jets where one of them is b-tagged. We can also tag a top quark if it is produced with large transverse momentum ( $p_T^{top} > m_{top}$ ). We identify the fat jet with  $R = 1.5$  and  $p_T > 200$  GeV using **HEPTopTagger** [22] with the following algorithm
  - Inside a fat jet, a loose massdrop criteria is employed such that  $J \rightarrow j_1 j_2$ ,  $m_{j_2} < m_{j_1}$  and  $m_{j_2} > 0.2m_J$ . The splitting takes place iteratively till  $m_{j_1} > 30$  GeV. A fat jet is retained if it has atleast three such subjets.
  - The three subjets are then filtered with  $\Delta R = 0.3$  into five subjets. Only those fatjets with total jet mass close to the top quark mass are considered. The subjets which reconstruct the top mass are then reclustered into three subjets.
  - These subjets are then required to satisfy decay kinematics. Among three pair of invariant mass with these subjets, two of them are independent (as one of them satisfies W-mass criteria). In a two dimensional space where the coordinates represent two independent invariant mass, top-like jets represent a thin

---

<sup>4</sup>To eliminate underlying events in the fatjet, it is filtered with  $R_{filter} = 0.3$  and three hard subjets are retained.

triangular annulus whereas QCD jet is localized in the region of small pair-wise invariant mass.

## 5.2 Signal-Background analysis

In this section, we discuss detailed signal and background analysis for the following channels viz.  $gg \rightarrow h \rightarrow \gamma\gamma$ ,  $Vh \rightarrow V\gamma\gamma$ ,  $Vh \rightarrow Vb\bar{b}$  and  $t\bar{t}h \rightarrow t\bar{t}b\bar{b}$  described in sec. 3. However, in  $Vh$  process, we will consider only  $Wh$  as the leptonic branching ratio is small in case of  $Z$ . We discuss the methods to suppress the backgrounds associated with the selected channels using the prescription of the object reconstruction defined in sec. 5.1.

### 5.2.1 Channel 1: $pp \rightarrow h \rightarrow \gamma\gamma$

We consider the decay of light Higgs ( $h$ ) with mass  $m_h$  to a pair of photons. The irreducible<sup>5</sup> diphoton background mainly comes from tree level quark-antiquark as well as loop induced gluon-gluon annihilation to  $\gamma\gamma$ . The reducible background arises from  $j\gamma$ ,  $jj$  and  $e^+e^-$  final states. The transverse momentum distribution for leading photon ( $p_T^\gamma$ ) corresponding to signal and SM backgrounds is plotted in fig. 5. While the  $p_T$  for the signal distribution peaks at approximately  $m_h/2$ , the backgrounds from  $\gamma\gamma$ ,  $j\gamma$  and  $jj$  peaks at lower values of  $p_T$  and hence can be reduced by giving a suitable  $p_T$  cut. Also since the photons produced from jets are not isolated,  $j\gamma$  and  $jj$  backgrounds can be suppressed further by selecting isolated photons. Although there is approximately 5% probability for an electron to fake a photon,  $Z$  pole contributions in Drell Yan background ( $Z \rightarrow ee$ ) process dilutes the signal. Since the  $p_T$  of such an electron faking as a photon is also hard (see fig. 5), putting a  $p_T$  cut on it is not efficient enough to reduce  $ee$  background around  $Z$  mass.

The analysis has been performed for 14 TeV center-of-mass energy at the LHC for  $m_h = 80, 90, 100$  and 110 GeV. To isolate signal from SM backgrounds, we demand presence of two isolated photons satisfying a mass dependent  $p_T$  criteria and having invariant mass ( $m_{\text{inv}}^{\gamma\gamma}$ ) within the window of 5 GeV centered about  $m_h$  i.e.,

$$p_{T_{\text{lead}}}^\gamma > \frac{m_h}{2} - 10 \text{ GeV}, p_{T_{\text{sub}}}^\gamma > \frac{m_h}{2} - 15 \text{ GeV}, |m_{\text{inv}}^{\gamma\gamma} - m_h| < 2.5 \text{ GeV}. \quad (5.1)$$

Clearly for larger values of  $m_h$ , the photons are produced with larger transverse momentum. The background reduction in such cases is significant which enables high chances of observing light Higgs. In fig. 6, we plot the significance<sup>6</sup>  $S(\gamma\gamma)$  of observing  $h$  with respect to  $\alpha$  for  $m_h = 100, 110$  GeV and integrated Luminosity,  $\mathcal{L} = 1000 \text{ fb}^{-1}$ . The significance for observing signal for  $m_h = 80, 90$  GeV is small, hence not shown in the plot. The dip in the fig. 6 corresponds to cases where  $\sigma(pp \rightarrow h \rightarrow \gamma\gamma) \approx (\xi_h^f)^2 \times (\xi_h^\gamma)^2$  vanishes (see fig. 10). While  $\xi_h^f \rightarrow 0$  in the fermiophobic limit i.e.  $\alpha \approx \pi/2$ ,  $\xi_h^\gamma \rightarrow 0$  when the contributions from top and  $W$  loop to  $h \rightarrow \gamma\gamma$  cancels. For large values of  $\tan\beta$ ,  $\alpha$

<sup>5</sup>There are mainly two types of backgrounds associated with a particular signal topology —reducible and irreducible. The irreducible background consists of exactly the same final state. Although the final state for the reducible backgrounds is somewhat different, it can contribute to the particular signal topology because of misidentification of the objects.

<sup>6</sup>  $S = s/\sqrt{s+b} \sim s/\sqrt{b}$  when  $s \ll b$

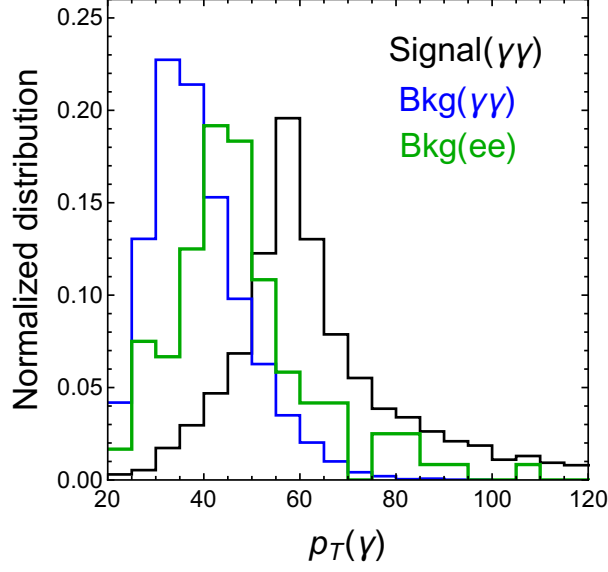


**Figure 5:** Plot showing  $p_T$  distribution for signal ( $m_h = 110$  GeV) and background ( $\gamma\gamma$  and  $ee$ ) for  $ggF \rightarrow h \rightarrow \gamma\gamma$  channel.

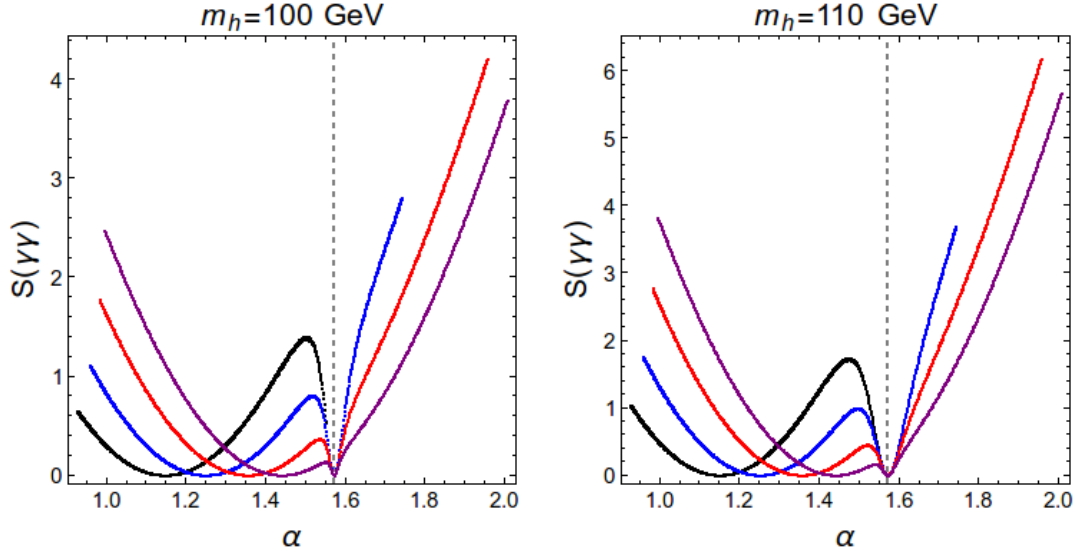


**Figure 6:** Significance in  $ggF \rightarrow h \rightarrow \gamma\gamma$  is shown with respect to  $\alpha$  for  $m_h = 100, 110$  GeV and  $\mathcal{L} = 1000 \text{ fb}^{-1}$ . Different colors corresponds to different values of  $\tan \beta$  : Black, blue, red and purple represents  $\tan \beta = 3, 4, 6$  and  $10$  respectively.

corresponding to  $\xi_h^\gamma \rightarrow 0$  shifts towards  $\pi/2$  (see eqn. 2.13). Note that the significance of observing the signal is larger for  $\alpha > \pi/2$  as  $\sin(\beta - \alpha) < 0$  and top and  $W$  loop interferes constructively which enhances the diphoton rate.

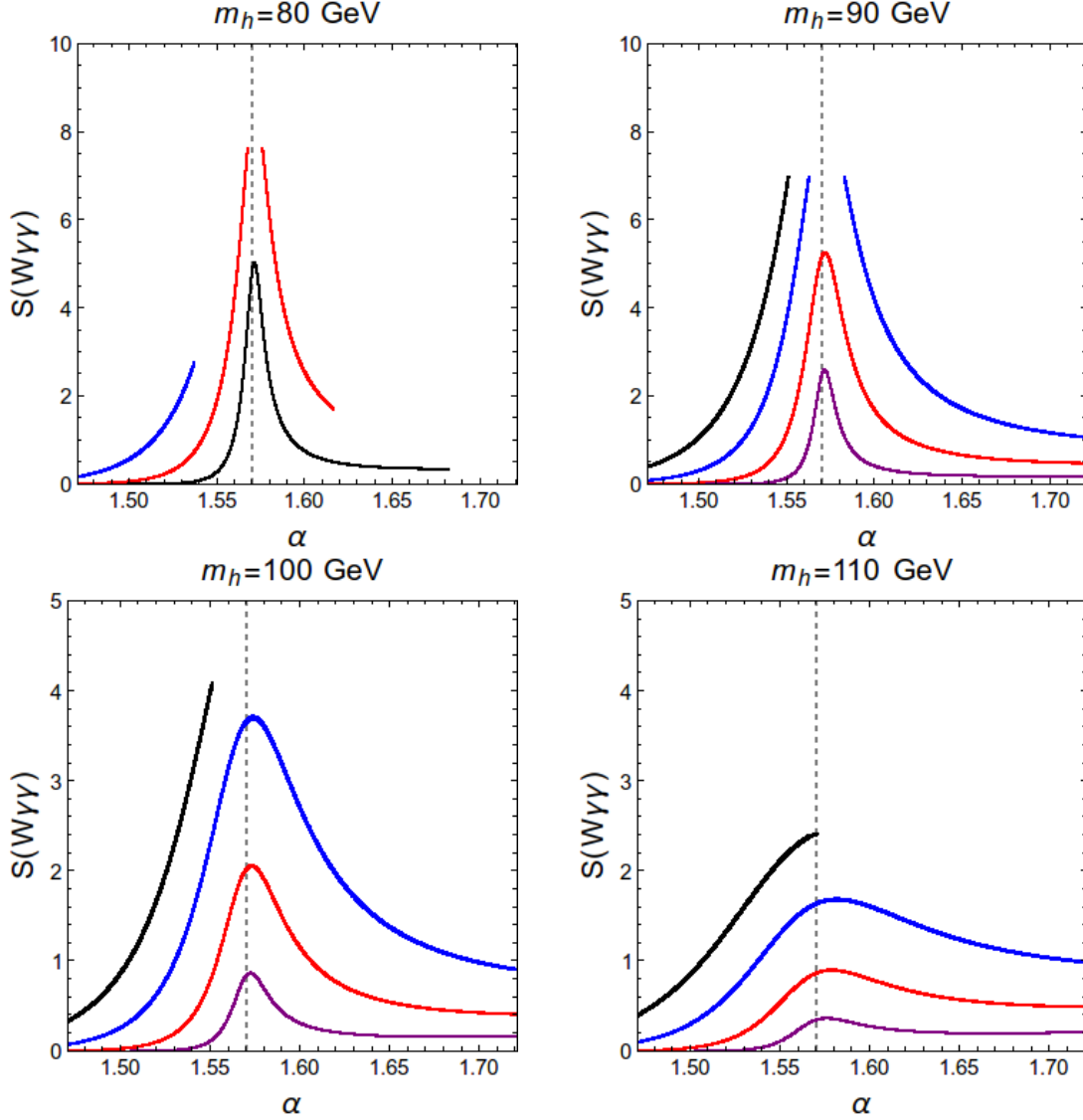


**Figure 7:** Significance of observing  $pp \rightarrow Wh \rightarrow \ell\nu\gamma\gamma$  is plotted with respect to  $\alpha$  for  $m_h = 80, 90, 100, 110$  GeV for  $\mathcal{L} = 100 \text{ fb}^{-1}$ . The color code is same as that in fig. 6.

### 5.2.2 Channel 2: $pp \rightarrow Wh \rightarrow \ell\nu\gamma\gamma$

This analysis is performed with 13 TeV center-of-mass energy at LHC in which  $W$  decays leptonically and light Higgs to diphoton. Hence, the signal is characterized by an isolated lepton, a pair of isolated photons and  $E_T^{\text{miss}} > 30 \text{ GeV}$ . The SM background comes primarily from the process  $pp \rightarrow W\gamma$ . We also consider  $Wj$  process as a potential background with jet faking a photon. The background can be suppressed by demanding isolated photon candidates. The probability of two electrons/jets faking two photons from the decay of  $Z$  in the process  $pp \rightarrow WZ$  has been taken into account as well. The following selection



criteria have been used:

$$p_{T\ell} > 30 \text{ GeV}, E_T^{\text{miss}} > 30 \text{ GeV}, p_{T_{\text{lead}}}^\gamma > m_h/2 - 10 \text{ GeV}, \\ p_{T_{\text{sub}}}^\gamma > m_h/2 - 15 \text{ GeV}, |m_{\text{inv}} - m_h| < 2.5 \text{ GeV}$$

As discussed earlier, the channel allows us to probe the fermiophobic limit where production via gluon fusion process loses its sensitivity. In the fig. 7, we have plotted the significance,  $S(\ell\nu\gamma\gamma)$ , of the signal with  $\alpha$  for  $50 \text{ fb}^{-1}$  integrated Luminosity for a fixed  $m_h$ . The significance is quite high for lower masses  $m_h = 80, 90 \text{ GeV}$  because the production cross section is higher for low masses,  $Z\gamma$  background is minuscule below  $Z$  resonance and this region is least constrained by the LHC data [18, 31]. For a given value of  $\tan\beta$  and  $m_h$ , the significance is maximum for  $\alpha \rightarrow \pi/2$ . Different lines on each plot represent various values of  $\tan\beta$ . For  $m_h = 80 \text{ GeV}$ , the line corresponding to  $\tan\beta = 4$  (blue) stops abruptly before reaching  $\alpha \sim \pi/2$  as the point beyond that is already ruled out by LEP search. The fermiophobic region ( $1.55 < \alpha < 1.6$ ) can be best explored with LHC 13 TeV centre of mass energy for  $\tan\beta = 6.0$  (red line). With further increment of  $\tan\beta$ , the magnitude of  $\sin(\beta - \alpha)$  comes down, thus, reducing  $Wh$  production cross section and hence, significance.

### 5.2.3 Channel 3: $pp \rightarrow Wh \rightarrow \ell\nu b\bar{b}$

We demand in this case two b-tagged jets, an isolated lepton along with  $E_T^{\text{miss}} > 30 \text{ GeV}$ . In spite of being the dominant decay channel in most of the parameter space,  $b\bar{b}$  mode is a difficult channel to probe due to enormous QCD background. As discussed in previous section, leptons and b-jets can only be tagged if they are produced with high transverse momentum and are central ( $|\eta| < 2.5$ ). Due to low mass of the  $Wh$  system, large fraction of b-jets and leptons could be produced with large  $|\eta|$ , thus, reducing the acceptance. Even if captured by the detector, they are accompanied by huge SM diboson backgrounds (primarily  $WZ$ ) and  $t\bar{t}$  (with one of the  $W$  along the beam line and escaping detection). In addition,  $W$ +jets poses a serious threat to signal with the jet faking as a b-jet. Moreover, the  $Wh$  production rate is governed by the magnitude of  $\xi_h^V$  and hence, is small in the favored parameter space. In the mass range we are considering it is nearly impossible to isolate signal events from huge SM backgrounds in  $2b + \ell + E_T^{\text{miss}}$  final state at the LHC.

In order to achieve appreciable significance at the LHC, we follow the analysis of [21] and consider  $Wh$  process in boosted regime. Though, we lose a significant number of events for demanding a boosted Higgs ( $p_T^h > 200 \text{ GeV}$ ), it enables us to overcome huge SM backgrounds quite efficiently. We reconstruct a fat jet with radius parameter  $\Delta R = 0.8$  and tag the fat jet as Higgs using the criteria discussed in section 5.1. The massdrop criteria along with double b-tag suppresses  $W$ +jets background. On demanding one isolated lepton and no jet activity outside the fat jet, we are able to suppress the  $t\bar{t}$  background as well. Therefore, we demand an isolated lepton and a fat jet in the final state. We then select only those events where the fat jet tagged as Higgs has filtered jet mass ( $m_J^{\text{Higgs}}$ ) lying around  $10 \text{ GeV}$  mass bin centered about  $m_h$ . We carried out the analysis with 14 TeV centre of mass energy for  $m_h = 70, 80, 100$  and  $110$ . We have not considered  $90 \text{ GeV}$  explicitly as

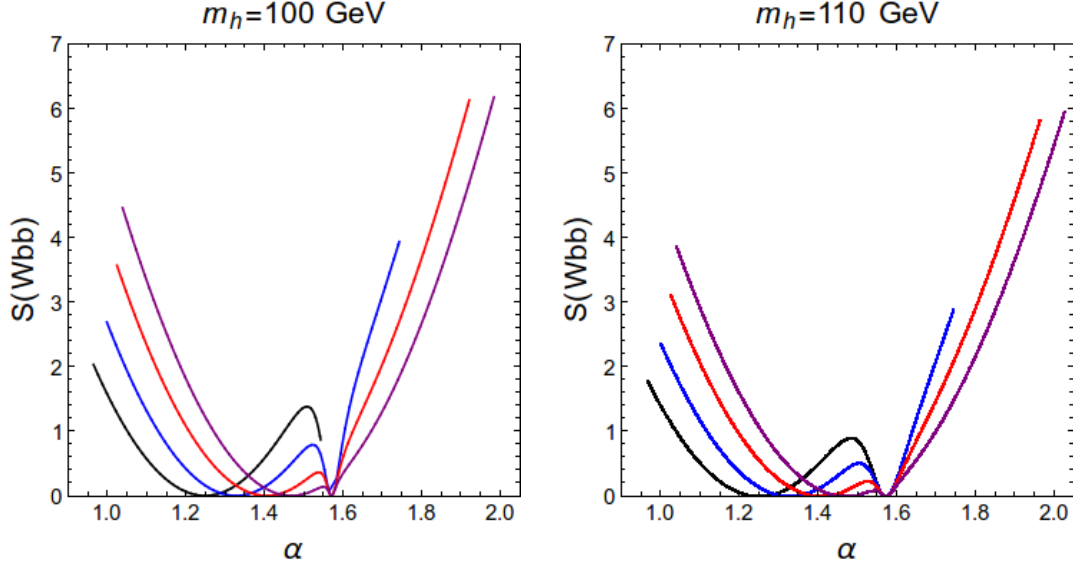


**Figure 8:** Variation of significance  $S(\ell\nu b\bar{b})$  in  $\ell\nu b\bar{b}$  channel with  $\alpha$  for different values of  $m_h$  at  $1000 \text{ fb}^{-1}$  integrated Luminosity. Points in black denote  $\tan \beta = 3$ , blue ( $\tan \beta = 4$ ), red ( $\tan \beta = 6$ ) and purple ( $\tan \beta = 10$ ).

near the Z-pole it will be difficult to isolate signal from  $Z \rightarrow b\bar{b}$  events. We summarize our selection criteria as:

$$p_T^\ell > 30 \text{ GeV}, E_T^{\text{miss}} > 30 \text{ GeV}, p_T^W = |\mathbf{p}_T^W| = |\mathbf{p}_T^\ell + \mathbf{p}_T^{\text{miss}}| > 200 \text{ GeV}$$

$$p_T^J > 200 \text{ GeV}, R_J = 0.8, |m_h - m_J| < 5.$$

$\mathbf{p}_T^W$  is the magnitude of vector sum of momentum of lepton and missing energy in the transverse plane. For  $m_h > 90 \text{ GeV}$ , we have reconstructed the fat jet with  $p_T > 250 \text{ GeV}$ . We have also selected events with  $|m_J - m_h| < 8 \text{ GeV}$ .

When  $m_h < 82 \text{ GeV}$ , the LEP direct detection measurements rule out  $|\xi_h^V| > 0.2$ . As the  $Wh$  production rate is small (apart from our cut criterion with large  $p_T$ ), the prospect of observing such a light Higgs is low even with  $3000 \text{ fb}^{-1}$  integrated Luminosity. The significance ( $S(\ell\nu b\bar{b})$ ) is plotted in fig. 8 as a function of  $\alpha$ . The left (right) panel of the figure represents significance with integrated Luminosity of  $1000 \text{ fb}^{-1}$  for  $m_h = 100$  (110) GeV. When  $m_h > 90 \text{ GeV}$ , LHC signal strength measurements rule out  $|\xi_h^V| > 0.3$  for  $\tan \beta < 3$ . Prospect of depicting light Higgs in this particular channel is limited for low  $\tan \beta$  due to small cross section. With higher value of  $\tan \beta$ , the constraint on maximum allowed value of  $\sin(\beta - \alpha)$  i.e.  $(|\xi_h^{Vmax}|)^7$  becomes weaker and hence, the significance increases. It is interesting to note the variation of signal significance from fig. 8. The dip in the plot signifies the points where the cross section  $(\sigma(Wh \rightarrow b\bar{b}) \propto \xi_h^V \times \xi_h^f)$  vanishes. The first dip corresponds to  $\xi_h^V \rightarrow 0$  and the second dip represents  $\xi_h^f \rightarrow 0$  (fermiophobic limit). The significance increases further as  $\alpha$  is moved away from fermiophobic (and fermiophilic)

<sup>7</sup> $\xi_h^{Vmax}$  is the maximum value of  $\sin(\beta - \alpha)$  allowed by LHC signal strength measurements.

point. Since LHC favors negative  $\sin(\beta - \alpha)$  over positive magnitude, the significance is slightly higher for negative  $\sin(\beta - \alpha)$ . Regions with  $\tan\beta > 4$  and  $\alpha > 1.8$  can be probed with  $1000 \text{ fb}^{-1}$  integrated Luminosity using  $\ell\nu b\bar{b}$  channel.

#### 5.2.4 Channel 4: $pp \rightarrow t\bar{t}h \rightarrow t\bar{t}b\bar{b}$

The analysis is carried out with 14 TeV centre of mass energy. We consider  $t\bar{t}h$  production with the Higgs decaying to  $b\bar{b}$  and semi-leptonic decay of the top pair<sup>8</sup>. The final state is composed of four bottom quarks, an isolated lepton and with  $E_T^{\text{miss}} > 30 \text{ GeV}$ . The irreducible background, in this case, is  $t\bar{t}b\bar{b}$  which appears at tree level with a  $W$  exchange. Another important background is  $t\bar{t} + \text{jets}$  where jet fakes the bottom quark. Due to presence of four b quarks in the final state, it is difficult to reconstruct the light Higgs accurately owing to several combinations. In the LHC run-II, top and the Higgs of  $t\bar{t}h$  process are produced with high transverse momentum and it is possible to study them in the boosted scenario. As a result, the decay product of (the hadronically decaying) top quark (and also the light Higgs) can be enclosed within a large radius that solves the problem arising from combinatorics. Therefore, our signal essentially becomes two fat jets and an isolated lepton. We reconstruct two fat jets with  $p_T^J > 125 \text{ GeV}$  and  $\Delta R = 1.2$ . Out of these two fat jets, we select the fat jet with  $p_T^J > 250 \text{ GeV}$  and tag it as top-jet following the prescription described in section 5.1. We then tag the other jet as the Higgs such that its filtered jet mass ( $m_J^{\text{Higgs}}$ ) lies within 10 GeV window about the light Higgs mass. The selection criteria are sufficient to suppress the irreducible background  $t\bar{t}b\bar{b}$ . However, there still exists configuration arising from  $t\bar{t} + \text{jets}$  where the bottom quark from leptonic top can go into the nearest fat jet and as a result the fat jet gets identified as Higgs. In order to get rid of such configuration we demand an anti-kt b-tagged jet outside the top-tagged fat jet and Higgs tagged fat jet. We summarize our selection criteria below

$$p_T^\ell > 30 \text{ GeV}, E_T^{\text{miss}} > 30 \text{ GeV}, p_T^J > 125 \text{ GeV} \text{ and } R_J = 1.2,$$

$$p_T^{\text{top}} > 250 \text{ GeV}, 150 \text{ GeV} < m_J^{\text{top}} < 200 \text{ GeV} \text{ and } |m_J^{\text{Higgs}} - m_h| < 5.$$

For  $m_h > 90 \text{ GeV}$ , we have reconstructed fat jets with  $p_T^J > 160 \text{ GeV}$  and selected events with  $|m_{Higgs}^J - m_h| < 8 \text{ GeV}$ .

In fig. 9 we have shown the variation of significance  $S(t\bar{t}b\bar{b})$  with  $\alpha$  for a given  $m_h$ . With increase in mass the significance decreases due to decrease in  $t\bar{t}h$  production rate. For a given mass, with increase in  $\tan\beta$ ,  $\xi_h^f$  decreases. Since, the total cross section gets scaled by  $(\xi_h^f)^4$ , the significance decreases. The significance is higher for lower values of  $\alpha$ . The channel is effective for probing lower  $\tan\beta$  region. This particular channel does not work out in the fermiophobic limit as both the production and decay become negligibly small.

---

<sup>8</sup>We have not considered 90 GeV as it will be difficult to isolate signal events from  $t\bar{t}Z$  background near the Z-pole

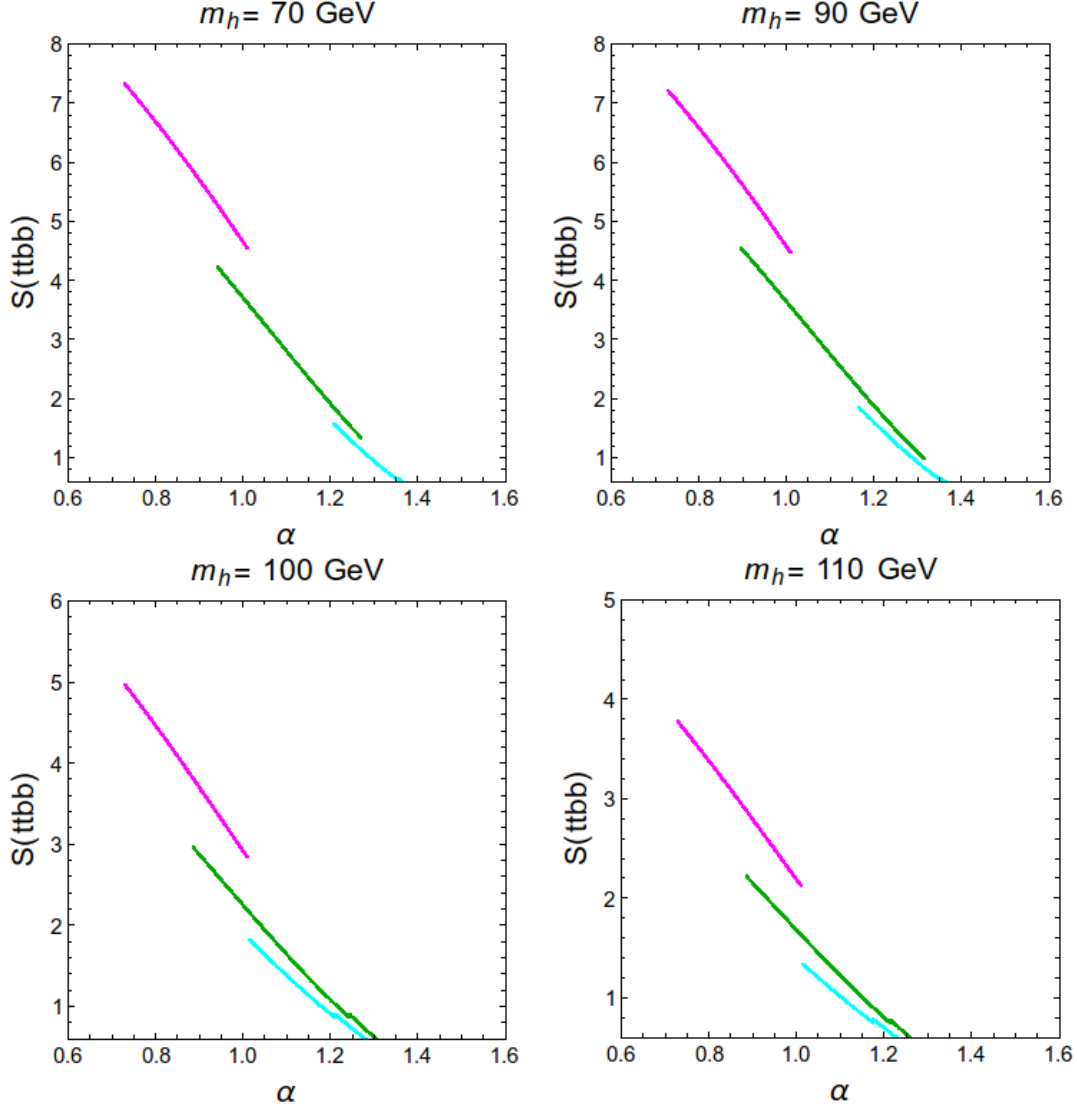


**Figure 9:** Variation of significance  $S(t\bar{t}b\bar{b})$  in the channel  $t\bar{t}b\bar{b}$  with  $\alpha$  for different values of  $m_h$  at  $1000 \text{ fb}^{-1}$  integrated Luminosity. Points in magenta denote  $\tan\beta = 1.2$ , green ( $\tan\beta = 2.0$ ), and cyan ( $\tan\beta = 5.0$ ).

## 6 Discussions and Conclusion

In this work, we focus on Type-I 2HDM with a Higgs lighter than the observed Higgs of mass 125 GeV. A light Higgs is still allowed from existing bounds and there are ongoing searches for such a Higgs at the LHC. We discuss various experimental constraints for such a scenario. The primary decay channel(s) of the light Higgs is  $b\bar{b}$  (and  $\tau\bar{\tau}$ ). But, in Type-I 2HDM, there are certain regions of parameter space where the Higgs becomes fermiophobic (and hence, diphoton decay mode becomes dominant). However,  $b\bar{b}$  faces serious challenge from QCD background, whereas, diphoton is much cleaner. Therefore, our aim in this study is to put together all such relevant information and provide an optimised search

strategy for such light Higgs scenario at the LHC.

$m_h$ (GeV)	$\tan \beta$	$\alpha^{\text{excluded}}$		Future Prospect		
		LEP + $\mu_{125}$	$\gamma\gamma$	$\alpha$	Channel	$\mathcal{L} \text{ fb}^{-1}$ (ECM)
70	1.2	$\alpha < 0.8, \alpha > 1.2$	–	0.8 – 0.9	ttbb	1000 (14)
	2.0	$\alpha < 0.9, \alpha > 1.3$	–	1.0 – 1.1	ttbb	3000 (14)
80	1.2	$\alpha < 0.7, \alpha > 1.1$	–	0.7 – 1.0	ttbb	1000 (14)
	2.0	$\alpha < 0.9, \alpha > 1.32$	–	1.0 – 1.1	ttbb	3000 (14)
	6.0	$\alpha < 1.2, \alpha > 1.61$	$\pi/2$	$ \pi/2 - \alpha  < 0.01$	$\ell\nu\gamma\gamma$	50 (13)
90	3.0	$\alpha < 0.92, \alpha > 1.55$	$\pi/2$	$> 1.54$	$\ell\nu\gamma\gamma$	50 (13)
	6.0	$\alpha < 1.0, \alpha > 1.8$	–	$ \pi/2 - \alpha  < 0.01$	$\ell\nu\gamma\gamma$	50 (13)
100	1.2	$\alpha < 0.7, \alpha > 1.0$	–	0.8 – 1.0	ttbb	3000 (14)
	4.0	$\alpha < 0.95, \alpha > 1.75$	–	$1.565 < \alpha < 1.584$	$\ell\nu\gamma\gamma$	100 (13)
	6.0	$\alpha < 0.97, \alpha > 1.96$	–	$> 1.8$	$\ell\nu b\bar{b}$	1000 (14)
110	1.2	$\alpha < 0.7, \alpha > 1.0$	–	0.7 – 0.9	ttbb	3000 (14)
	4.0	$\alpha < 0.95, \alpha > 1.75$	–	$1.563 < \alpha < 1.60$	$\ell\nu\gamma\gamma$	500 (14)
	6.0	$\alpha < 0.97, \alpha > 1.96$	–	$> 1.9$	$\gamma\gamma$	1000 (14)

**Table 4:** We tabulate the regions of  $\alpha$  which can be probed with at least  $5\sigma$  significance for a fixed mass and  $\tan \beta$ . For example,  $1.56 < \alpha < 1.58$  for  $m_h = 80$  GeV and  $\tan \beta = 6.0$  can be probed best in  $pp \rightarrow Wh \rightarrow \ell\nu\gamma\gamma$  channel at 13 TeV run of LHC with integrated Luminosity  $50 \text{ fb}^{-1}$ . We also list the regions of  $\alpha$  excluded from LEP as well as signal strength measurements of SM-like Higgs at LHC.

We summarize our results in Table 4. Here  $\alpha_{\text{excluded}}$  denotes the regions which are already ruled out by various experimental data from LEP and LHC. The column on the right side represents the region of  $\alpha$  that can be probed in the run-II of the LHC. Gluon fusion is the main production channel of light Higgs just like in case of SM-like Higgs. However, gluon fusion cross section drops significantly in the fermiophobic limit and hence, associated productions or VBF turns out to be important supplier. Note that our choice of production and decay channels are complimentary in probing the parameter space. The fermiophobic region ( $\alpha \rightarrow \pi/2$ ) can be best probed by  $pp \rightarrow Wh \rightarrow \ell\nu\gamma\gamma$  at the 13 TeV LHC with  $50 \text{ fb}^{-1}$  integrated Luminosity. Away from the fermiophobic region,  $pp \rightarrow t\bar{t}h \rightarrow t\bar{t}b\bar{b}$  seems to be the best channel at low  $\tan \beta$  with at least  $1000 \text{ fb}^{-1}$  Luminosity at 14 TeV LHC. In this case, boosted technique can tackle huge QCD multijet background effectively. For higher  $\tan \beta$ ,  $pp \rightarrow h \rightarrow \gamma\gamma$  turns out to be the efficient channel at  $1000 \text{ fb}^{-1}$  Luminosity at 14 TeV LHC.

We must mention that our analysis is more or less generic, in the sense, that it would hold true for any other scenario with lighter Higgs. LHC will continue its hunt for new physics. The absence of any significant excess over SM backgrounds so far has provoke us to explore higher energy scale. We demonstrate a possible scenario where BSM particles lighter than the observed Higgs is buried beneath the SM background and can be probed in

ensuing run of LHC. The discovery of such a Higgs would definitely help us to understand the electroweak symmetry breaking mechanism.

## 7 Acknowledgement

We would like to thank Sandhya Jain for helpful discussions. We would also like to acknowledge Sreerup Raychaudhuri for carefully reading the manuscript. SN acknowledges Dr. D. S. Kothari Post Doctoral Fellowship awarded by University Grant Commission (award letter no. PH/15-16/0073) for financial support. We would also like to thank Department of Theoretical Physics, TIFR for the use of its computational resources.

## A Cross-section plots

The behaviour of the total cross-sections with respect to  $\alpha$  and  $\sin(\beta - \alpha)$  for different values of  $\beta$  is plotted in fig. 10

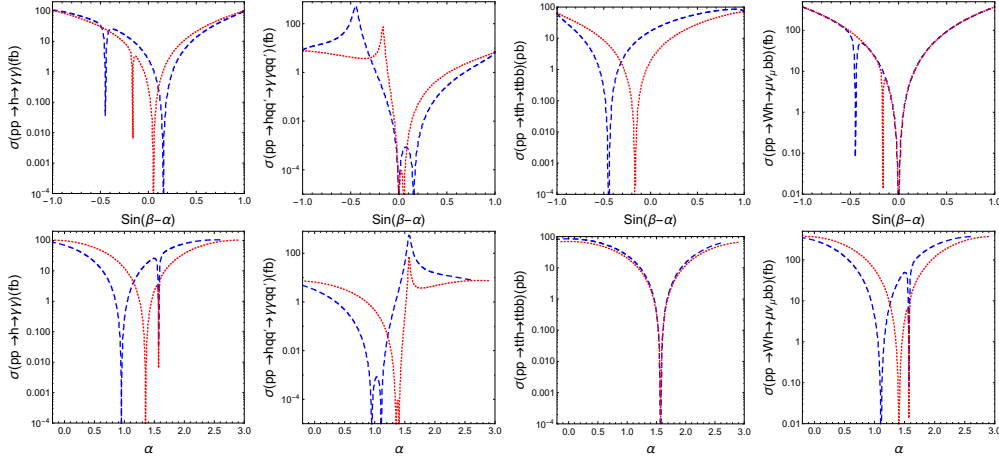


**Figure 10:** A representative plot for  $m_h = 90$  GeV. The dashed line in blue corresponds to  $\tan \beta = 2$  while the dotted line in red corresponds to a  $\tan \beta = 6$ .

## References

- [1] **ATLAS** Collaboration, G. Aad et al., *Observation of a new particle in the search for the Standard Model Higgs boson with the ATLAS detector at the LHC*, *Phys. Lett.* **B716** (2012) 1–29, [[arXiv:1207.7214](#)].
- [2] **CMS** Collaboration, S. Chatrchyan et al., *Observation of a new boson at a mass of 125 GeV with the CMS experiment at the LHC*, *Phys. Lett.* **B716** (2012) 30–61, [[arXiv:1207.7235](#)].
- [3] **ATLAS, CMS** Collaboration, G. Aad et al., *Measurements of the Higgs boson production and decay rates and constraints on its couplings from a combined ATLAS and CMS analysis of the LHC pp collision data at  $\sqrt{s} = 7$  and 8 TeV*, *JHEP* **08** (2016) 045, [[arXiv:1606.02266](#)].

- [4] G. C. Branco, P. M. Ferreira, L. Lavoura, M. N. Rebelo, M. Sher, and J. P. Silva, *Theory and phenomenology of two-Higgs-doublet models*, *Phys. Rept.* **516** (2012) 1–102, [[arXiv:1106.0034](#)].
- [5] C.-W. Chiang and K. Yagyu, *Implications of Higgs boson search data on the two-Higgs doublet models with a softly broken  $Z_2$  symmetry*, *JHEP* **07** (2013) 160, [[arXiv:1303.0168](#)].
- [6] O. Eberhardt, U. Nierste, and M. Wiebusch, *Status of the two-Higgs-doublet model of type II*, *JHEP* **07** (2013) 118, [[arXiv:1305.1649](#)].
- [7] S. Inoue, M. J. Ramsey-Musolf, and Y. Zhang, *CP-violating phenomenology of flavor conserving two Higgs doublet models*, *Phys. Rev.* **D89** (2014), no. 11 115023, [[arXiv:1403.4257](#)].
- [8] N. Craig, J. Galloway, and S. Thomas, *Searching for Signs of the Second Higgs Doublet*, [[arXiv:1305.2424](#)].
- [9] C.-Y. Chen, S. Dawson, and M. Sher, *Heavy Higgs Searches and Constraints on Two Higgs Doublet Models*, *Phys. Rev.* **D88** (2013) 015018, [[arXiv:1305.1624](#)]. [Erratum: *Phys. Rev.* **D88**, 039901(2013)].
- [10] A. Arhrib, P. M. Ferreira, and R. Santos, *Are There Hidden Scalars in LHC Higgs Results?*, *JHEP* **03** (2014) 053, [[arXiv:1311.1520](#)].
- [11] A. Celis, V. Ilisie, and A. Pich, *Towards a general analysis of LHC data within two-Higgs-doublet models*, *JHEP* **12** (2013) 095, [[arXiv:1310.7941](#)].
- [12] A. Celis, V. Ilisie, and A. Pich, *LHC constraints on two-Higgs doublet models*, *JHEP* **07** (2013) 053, [[arXiv:1302.4022](#)].
- [13] J. F. Gunion and H. E. Haber, *The CP conserving two Higgs doublet model: The Approach to the decoupling limit*, *Phys. Rev.* **D67** (2003) 075019, [[hep-ph/0207010](#)].
- [14] S. Chang, S. K. Kang, J.-P. Lee, K. Y. Lee, S. C. Park, and J. Song, *Two Higgs doublet models for the LHC Higgs boson data at  $\sqrt{s} = 7$  and 8 TeV*, *JHEP* **09** (2014) 101, [[arXiv:1310.3374](#)].
- [15] B. Dumont, J. F. Gunion, Y. Jiang, and S. Kraml, *Constraints on and future prospects for Two-Higgs-Doublet Models in light of the LHC Higgs signal*, *Phys. Rev.* **D90** (2014) 035021, [[arXiv:1405.3584](#)].
- [16] J. Bernon, J. F. Gunion, Y. Jiang, and S. Kraml, *Light Higgs bosons in Two-Higgs-Doublet Models*, *Phys. Rev.* **D91** (2015), no. 7 075019, [[arXiv:1412.3385](#)].
- [17] S. Chang, S. K. Kang, J.-P. Lee, and J. Song, *Higgs potential and hidden light Higgs scenario in two Higgs doublet models*, *Phys. Rev.* **D92** (2015), no. 7 075023, [[arXiv:1507.03618](#)].
- [18] G. Cacciapaglia, A. Deandrea, S. Gascon-Shotkin, S. Le Corre, M. Lethuillier, and J. Tao, *Search for a lighter Higgs boson in Two Higgs Doublet Models*, *JHEP* **12** (2016) 068, [[arXiv:1607.08653](#)].
- [19] CMS Collaboration, V. Khachatryan et al., *Limits on the Higgs boson lifetime and width from its decay to four charged leptons*, *Phys. Rev.* **D92** (2015), no. 7 072010, [[arXiv:1507.06656](#)].
- [20] L. Brucher and R. Santos, *Experimental signatures of fermiophobic Higgs bosons*, *Eur. Phys. J.* **C12** (2000) 87–98, [[hep-ph/9907434](#)].



- [21] J. M. Butterworth, A. R. Davison, M. Rubin, and G. P. Salam, *Jet substructure as a new Higgs search channel at the LHC*, *Phys. Rev. Lett.* **100** (2008) 242001, [[arXiv:0802.2470](#)].
- [22] T. Plehn and M. Spannowsky, *Top Tagging*, *J. Phys.* **G39** (2012) 083001, [[arXiv:1112.4441](#)].
- [23] D. Eriksson, J. Rathsmann, and O. Stal, *2HDMC: Two-Higgs-doublet model calculator*, *Comput. Phys. Commun.* **181** (2010) 833–834.
- [24] J. F. Gunion, H. E. Haber, G. L. Kane, and S. Dawson, *The Higgs Hunter’s Guide*, *Front. Phys.* **80** (2000) 1–404.
- [25] F. Mahmoudi and O. Stal, *Flavor constraints on the two-Higgs-doublet model with general Yukawa couplings*, *Phys. Rev.* **D81** (2010) 035016, [[arXiv:0907.1791](#)].
- [26] A. Arbey and F. Mahmoudi, *SuperIso Relic v3.0: A program for calculating relic density and flavour physics observables: Extension to NMSSM*, *Comput. Phys. Commun.* **182** (2011) 1582–1583.
- [27] **OPAL, DELPHI, L3, ALEPH, LEP Higgs Working Group for Higgs boson searches** Collaboration, *Search for charged Higgs bosons: Preliminary combined results using LEP data collected at energies up to 209-GeV*, in *Lepton and photon interactions at high energies. Proceedings, 20th International Symposium, LP 2001, Rome, Italy, July 23-28, 2001*, 2001. [hep-ex/0107031](#).
- [28] **DELPHI, OPAL, ALEPH, LEP Working Group for Higgs Boson Searches, L3** Collaboration, S. Schael et al., *Search for neutral MSSM Higgs bosons at LEP*, *Eur. Phys. J.* **C47** (2006) 547–587, [[hep-ex/0602042](#)].
- [29] **DELPHI** Collaboration, P. Abreu et al., *Search for a fermiophobic Higgs at LEP-2*, *Phys. Lett.* **B507** (2001) 89–103, [[hep-ex/0104025](#)].
- [30] S. Dawson et al., *Working Group Report: Higgs Boson*, in *Proceedings, 2013 Community Summer Study on the Future of U.S. Particle Physics: Snowmass on the Mississippi (CSS2013): Minneapolis, MN, USA, July 29-August 6, 2013*, 2013. [arXiv:1310.8361](#).
- [31] **CMS** Collaboration, *Search for new resonances in the diphoton final state in the mass range between 80 and 110 GeV in pp collisions at  $\sqrt{s} = 8$  TeV*, Tech. Rep. CMS-PAS-HIG-14-037, CERN, Geneva, 2015.
- [32] **ATLAS** Collaboration, G. Aad et al., *Search for scalar diphoton resonances in the mass range 65–600 GeV with the ATLAS detector in pp collision data at  $\sqrt{s} = 8$  TeV*, *Phys. Rev. Lett.* **113** (Oct, 2014) 171801.
- [33] T. Sjostrand, S. Mrenna, and P. Z. Skands, *A Brief Introduction to PYTHIA 8.1*, *Comput. Phys. Commun.* **178** (2008) 852–867, [[arXiv:0710.3820](#)].
- [34] T. Sjostrand, S. Ask, J. R. Christiansen, R. Corke, N. Desai, P. Ilten, S. Mrenna, S. Prestel, C. O. Rasmussen, and P. Z. Skands, *An Introduction to PYTHIA 8.2*, *Comput. Phys. Commun.* **191** (2015) 159–177, [[arXiv:1410.3012](#)].
- [35] J. Alwall, R. Frederix, S. Frixione, V. Hirschi, F. Maltoni, O. Mattelaer, H. S. Shao, T. Stelzer, P. Torrielli, and M. Zaro, *The automated computation of tree-level and next-to-leading order differential cross sections, and their matching to parton shower simulations*, *JHEP* **07** (2014) 079, [[arXiv:1405.0301](#)].
- [36] S. Hoeche, F. Krauss, N. Lavesson, L. Lonnblad, M. Mangano, A. Schalicke, and S. Schumann, *Matching parton showers and matrix elements*, in *HERA and the LHC: A*



*Workshop on the implications of HERA for LHC physics: Proceedings Part A*, pp. 288–289, 2005. [hep-ph/0602031](#).

- [37] M. Cacciari, G. P. Salam, and G. Soyez, *The Anti- $k(t)$  jet clustering algorithm*, *JHEP* **04** (2008) 063, [[arXiv:0802.1189](#)].
- [38] M. Cacciari, G. P. Salam, and G. Soyez, *FastJet User Manual*, *Eur. Phys. J.* **C72** (2012) 1896, [[arXiv:1111.6097](#)].
- [39] S. Bentvelsen and I. Meyer, *The Cambridge jet algorithm: Features and applications*, *Eur. Phys. J.* **C4** (1998) 623–629, [[hep-ph/9803322](#)].